ACCSCIENCE PUBLISHING

International Journal of Bioprinting

RESEARCH ARTICLE

Optimizing printability and mechanical properties of poly(3-hydroxybutyrate) biocomposite blends and their biological response to Saos-2 cells

Štěpán Krobot[1]*, Přemysl Menčík[1], Kateřina Chaloupková[1], Ján Bočkaj[2], Sára Vach Agócsová[2], Michala Klusáček Rampichová[3], Věra Hedvičáková[3], Pavol Alexy[2], Radek Přikryl[1], and Veronika Melčová[1]*

[1]Institute of Material Chemistry, Faculty of Chemistry, Brno University of Technology, Brno, Czech Republic

[2]Faculty of Chemical and Food Technology, Institute of Natural and Synthetic Polymers, Slovak University of Technology in Bratislava, Bratislava, Slovakia

[3]Institute of Experimental Medicine, Czech Academy of Sciences, Prague, Czech Republic

(This article belongs to the Special Issue: *3D Printing for Tissue Engineering and Regenerative Medicine-Series 2*)

Abstract

Bone tissue engineering requires scaffolds with three-dimensional (3D) structures that facilitate vascularization and new tissue growth. 3D printing, especially through fused deposition modeling (FDM), has emerged as an effective method for creating complex structures with high reproducibility. Early research in this area demonstrated the potential of poly(ε-caprolactone) (PCL) and poly(L-lactide) (PLLA) scaffolds for bone regeneration. Recently, polylactide (PLA) and polyhydroxyalkanoates (PHAs) have garnered attention for their biocompatibility and ability to support cell proliferation. Among PHAs, poly(3-hydroxybutyrate) (PHB) shows promise due to its intrinsic biocompatibility and resorbability, making it a candidate for FDM-based scaffold fabrication. In the presented study, we aim to develop and optimize a biocompatible PHB-based composite material for bone tissue engineering, incorporating PLA, hydroxyapatite, and the plasticizer Syncroflex 3114 to enhance mechanical properties and printability. This composite was processed into filaments for 3D printing and characterized through thermal, mechanical, and biological evaluations. Using a design of experiment approach, we investigated factors such as temperature performance, warping, degradation, and strength to determine the optimal composition for use in tissue engineering. Four optimal mixture compositions fulfilling the optimization criteria of having the most suitable properties for bone tissue engineering, namely the best printability and maximum mechanical properties, were obtained. The mixtures were optimized specifically for minimum warping coefficient (0.5); maximum flexural strength (66.9 MPa); maximum compression modulus (2.4 GPa); and maximum compression modulus (2.3 GPa) with a warping coefficient of no more than 1 at the same time. In conclusion, the study shows a new possible way to effectively develop and test 3D-printed PHB-based scaffolds with specifically optimized material properties.

Keywords: 3D printing; Design of experiment; Fused deposition modeling; Poly(3-hydroxybutyrate); Polylactide; Printability; Scaffold

***Corresponding authors:**
Štěpán Krobot
(Stepan.Krobot@vutbr.cz)

Veronika Melčová
(xcmelcova@fch.vut.cz)

Citation: Krobot S, Menčík P, Chaloupková K, et al. Optimizing printability and mechanical properties of poly(3-hydroxybutyrate) biocomposite blends and their biological response to Saos-2 cells. *Int J Bioprint*. 2025;11(1):400-417. doi: 10.36922/ijb.5175

Received: October 16, 2024
Revised: November 10, 2024
Accepted: December 3, 2024
Published Online: December 4, 2024

Copyright: © 2024 Author(s). This is an Open Access article distributed under the terms of the Creative Commons Attribution License, permitting distribution, and reproduction in any medium, provided the original work is properly cited.

Publisher's Note: AccScience Publishing remains neutral with regard to jurisdictional claims in published maps and institutional affiliations.

1. Introduction

Among the broad range of requirements for bone tissue engineering scaffolds, having a suitable three-dimensional (3D) structure allowing vascularization and growth of the new tissue stands as an important criterion.[1] This can be achieved by 3D printing, which offers effective production of complex structures with high reproducibility.[2–4] Nowadays, the most common 3D printing technique is fused deposition modeling (FDM), which can be exploited for biopolymers as well.[5–9]

The first FDM-printed scaffolds for bone tissue engineering emerged in 2001. Hutmacher et al.[10] 3D-printed poly(ε-caprolactone) (PCL) scaffolds with honeycomb and lay-down pattern structures featuring good adhesion and proliferation of human fibroblasts and osteoprogenitor cells and a compression stiffness of 42 MPa. Xiong et al.[11] fabricated poly(L-lactide) (PLLA) grid structures with a compression yield strength of 8 MPa. Further research in this field was focused on the thorough characterization of scaffold properties or performance tuning by (1) the addition of bioactive filler; (2) blending with other biopolymers; (3) change of internal 3D structure; or (4) surface modifications.

Regarding PCL, the mechanical properties of 3D-printed scaffolds with varying porosity and pore size have been described.[12–15] Also, a composite of PCL with bioactive glass was found to be printable and showed higher proliferation of human fibroblasts and increased compressive modulus than neat polymer.[16] Nevertheless, the most studied PCL-based material for FDM 3D printing is composite with tricalcium phosphate (TCP).[17–21] This material was subjected to tests *in vivo*, for example on rat critical-sized femoral defect model by Rai et al.[18] and on porcine mandibular defects by Konopnicki et al.[20] Currently, the material is approved for humans in the craniofacial region[22] and is commercially available.[23]

As for polylactide (PLA), the progress in the field of bone replacement prepared by all 3D printing techniques has been reviewed by Chen et al.[24] PLA scaffolds show biocompatibility and suitable viability and proliferation of osteosarcoma cells[25] and higher viability of human osteoblasts (hFOB) than titanium sample.[26] In terms of mechanical properties, the gyroid structure is currently in the spotlight.[27–29] First described in 1970 by Schoen,[30] it has an open porosity and high strength per weight. The possibility of printing PLA composites with bioactive inorganics, such as TCP,[31–33] bioactive glass,[34] and mostly hydroxyapatite (HA),[35–40] has also been reported. Matsuo et al.[35] observed better bone healing for a PLLA with 50 wt% HA in two patients with mandibular injuries than with titanium.

Another interesting group of materials often exploited for tissue engineering are polyhydroxyalkanoates (PHA).[41] PHA has been utilized in the field of FDM-printed scaffolds for bone replacement from the start and often acts as a secondary polymer in the blend with PCL[42] or PLA[43–49] nowadays. In the last years, successful attempts at FDM printing of materials with a PHA majority emerged. One such example is poly(3-hydroxybutyrate-co-3-hydroxyhexanoate) (PHBH). In 2020, a PHBH composite containing acetylated nanocellulose with improved thermomechanical properties[50] and PHBH scaffolds compatible with mouse 3T3 fibroblast cells and degradable in synthetic gastric juice[51] were reported. In 2022, Dong et al.[52] created and seeded PHBH structures with costal cartilage and tested for a nipple reconstruction *in vivo* with promising results. The mechanical properties of PHBH scaffolds were characterized as well.[53,54] Another example is poly(3-hydroxybutyrate-co-3-hydroxyvalerate) (PHBV) and 3D-printed scaffolds from its composite with bioglass, which are compatible with mouse preosteoblasts MC3T3-E1 cells.[55] Ye et al. demonstrated a PHA filled with up to 30 wt% of TCP featuring a compressive strength of 37 MPa, which showed improved response of MC3T3-E1 cells compared to non-filled PHA. However, the type of PHA used was not specified.[56]

Last but not least, poly(3-hydroxybutyrate) (PHB) biopolymer offers intrinsic biocompatibility and resorbability which also applies to its degradation products. Moreover, PHB stands out with the mechanical properties appropriate to the replacement of hard tissue.[57–60] Thermal instability and the complex processability of PHB pose a major challenge for FDM. Therefore, PHB was first printed by selective laser sintering (SLS) method by Pereira et al.[61] To our knowledge, FDM-printed blends with most PHB majority for tissue engineering are scarcely described in the literature, except for publications stemmig from our research group.[62,63] Kanabenja et al.[64] prepared a PHB/PLA 70/30 blend plasticized with polypropylene glycol (PPG) with different dosages of HA and characterized its thermomechanical properties, crystal structure, and flowability. Moroni et al. [65] verified the possibility of using PHB for 3D printing by direct powder extrusion one-step method. Moreover, PHB was loaded with a model drug up to 30 wt% and tested for a prolonged release for 20 days.

In this study, we aim to characterize the important thermal, mechanical, and biological properties of the plasticized material PHB/PLA filled with HA across a range of compositions applicable to FDM 3D printing. The novelty of this research is the use of an innovative

biocomposite material whose composition can be tailored to the desired properties. Using the design of the experiment method, we also aim to identify the composition of optimized material for tissue engineering of bones and predict its properties. The polymer matrix consisted of predominantly PHB, supplemented with a smaller proportion of PLA. PHB was chosen due to its inherent biocompatibility, biodegradability, suitable processability, and mixability with other biopolymers for improved properties.

2. Materials and methods

2.1. Materials

Polymer mixtures contained poly(3-hydroxybutyrate) (PHB) EDW 2394 from TianAn (Ningbo City, China) and amorphous poly(D,L-lactide) (PLA) Ingeo™ Biopolymer 4060D from NatureWorks (Minnetonka, MN, USA). The used plasticizer is Syncroflex™ 3114 (abbreviated as SN) from Croda (Rawcliff, UK). Bioactive ceramics hydroxyapatite/tricalcium phosphate blend (abbreviated as HA) from AppliChem (Darmstadt, Germany) with D_{50} = 2.8 μm was used for the blends of the design of experiments.

2.2. Design of experiment

In order to find the optimal proportions of the components of the PHB/PLA/SN/HA mixture, a 3-factor, 5-level Design of Experiment (DoE) test was conducted. The factors and their limits were set as follows:

- Factor 1; x_1 = PLA/PHB ranged from 5/95 to 50/50 so that most of the PHB content added is retained;
- Factor 2; x_2 = HA/(PHB+PLA) ranged from 5/95 to 30/70 due to expected limits in processability;
- Factor 3; x_3 = SN/(PHB+PLA+HA), the SN content in the whole mixture ranged from 5.6 to 12.4 wt%.

Factor 1 corresponds to the polymer matrix of the material which is the basis for the 3D-printed specimen. The ratio of PHB/PLA thus reflects the retainment of PHB in the mixture. Factor 2 corresponds to the addition of the bioactive filler to the matrix. In theory and under ideal conditions, an larger amount of filler added would lead to a better biological response. Factor 3 corresponds to the addition of the plasticizer to the matrix because a larger amount of plasticizer added is associated with better processability of the material and smoother process of 3D printing.

Real values and steps of the experiment for coded levels are listed in Table 1. The real limit values in coded levels −1.682 and 1.682 correspond with the borderline composition of the samples described above. The middle value of the factor is located on the coded coordinate 0. The confidence interval was 95%.

2.2.1. Sample composition

Subsequently, the mathematical matrix of samples with assigned coordinates in coded levels was created. The composition of individual mixtures (referred to as Mix 1–Mix 20) was calculated from the assigned coded levels using real values in Table 1. The actual composition of all prepared samples is given in Table 2. Mixtures 9–14 contain limit values of one of the factors while the rest of the factors are located at the middle value. In other words, on these mixtures, we can observe the effect of the maximum/minimum content of individual mixture components in the tested range on measured properties. The samples Mix 15–20 have all the factors in coded level 0, in the middle of the composition range. These samples are included to provide the statistical error of the measurement.

2.2.2. Results evaluation

Measured data were fitted with a 3D curve given by the following equation:

$$y = b_0 + b_1x_1 + b_2x_2 + b_3x_3 + b_{11}x_1^2 + b_{22}x_2^2 + b_{33}x_3^2 + b_{12}x_1x_2 + b_{13}x_1x_3 + b_{23}x_2x_3, \quad (1)$$

where x_{1-3} are factors of the experiment and b_{ij} are coefficients indexed with numbers 1–3 according to the DoE factor they relate to. The coefficients b_{1-3} indicate the degree of linear dependence of the measured parameter on the corresponding factor. The coefficients b_{11-33} give the degree of quadratic dependence of the measured

Table 1. Values of DoE in coded and real levels.

	Real values of the experiment					
Coded levels	**−1.682**	**−1**	**0**	**1**	**1.682**	**Step**
x_1 PLA/PHB	0.0526	0.2447	0.5263	0.8079	1.0000	0.2816
x_2 HA/(PHB+PLA)	0.0526	0.1288	0.2406	0.3524	0.4286	0.1118
x_3 SN/(PHB+PLA+HA)	0.0593	0.0760	0.1004	0.1249	0.1416	0.0244

Abbreviations: DoE, design of experiment; HA, hydroxyapatite; PHB, poly(3-hydroxybutyrate); PLA, polylactide; SN, Syncroflex™ 3114.

Table 2. Prepared samples with their composition in coded levels and respective weight fractions

	Factors in coded Levels			The actual composition			
Sample name	PLA/PHB	HA/ (PHB+PLA)	SN/ (PHB+PLA+HA)	PHB (wt%)	PLA (wt%)	SN (wt%)	HA (wt%)
Mix 1	−1	−1	−1	66	16	7	11
Mix 2	1	−1	−1	46	37	7	11
Mix 3	−1	1	−1	55	14	7	24
Mix 4	1	1	−1	38	31	7	24
Mix 5	−1	−1	1	63	15	11	10
Mix 6	1	−1	1	44	35	11	10
Mix 7	−1	1	1	53	13	11	23
Mix 8	1	1	1	36	29	11	23
Mix 9	−1.682	0	0	70	4	9	18
Mix 10	1.682	0	0	37	37	9	18
Mix 11	0	−1.682	0	57	30	9	5
Mix 12	0	1.682	0	42	22	9	27
Mix 13	0	0	−1.682	50	26	6	18
Mix 14	0	0	1.682	46	24	12	17
Mix 15–20	0	0	0	48	25	9	18

Abbreviations: HA, hydroxyapatite; PHB, poly(3-hydroxybutyrate); PLA, polylactide; SN, Syncroflex™ 3114.

parameter on the corresponding factor. Last but not least, the coefficients $b_{12/13/23}$ quantify the mutual effect of two factors. Statistical analysis of standard deviations of the results yields all coefficients together with their statistical relevance. Measured data are represented as 3D graphs, with two of the most statistically relevant factors on axes x and y. The third factor was fixed at a constant level.

2.3. Filament preparation

A total of 700 g of all mixtures was prepared. Compounding was performed with the corotating meshing twin screw extruder from Labtech Engineering Company (Samutprakarn, Thailand) with a screw diameter of 16 mm and length (L) diameter (D) ratio (L/D) of 40. The temperature setting from hopper to nozzle was: 60-120-180-190-190-190-170-160-160°C and the used rotations were 150 rpm. Granules were fed into a single screw extruder HAAKE Rheomex OS (Haake Technik GmbH, Vreden, Germany) with a screw diameter of 19 mm and an L/D of 30 and extruded into the form of 3D printing filaments. The temperature setting from hopper to nozzle was: 180-185-180-170°C for all samples except for Mix 5, 6 and 11, where the second heating zone setting was at 190°C. Rotations were set to 20 rpm. The filament diameter of 1.75 mm was controlled during the whole extrusion process.

2.4. Thermal properties

Basic thermal characterization was performed with differential scanning calorimetry (DSC) using DSC 2500 from TA Instrument (New Castle, DE, USA). The samples weighing 10–14 mg were hermetically sealed in aluminum pans and subjected to two heating cycles from −30 to 200°C with a 10°C·min^{-1} heating/cooling rate under a nitrogen atmosphere (50 mL·min^{-1}).

2.5. 3D printing

FDM 3D printer Original Prusa i3 MK3s (Prusa Research a.s., Prague, Czech Republic) was used with a nozzle with a standard diameter of 0.4 mm, controlled by the V3.9.0 firmware version manufactured by Prusa Research a.s. (Prague, Czech Republic). Another relevant setting of the printer is the printed layer height and width of 0.2 mm and 0.45 mm, respectively; the perimeter printing speed of 45 mm·s^{-1}; and the infill printing speed of 200 mm·s^{-1}. G-codes were prepared in PrusaSlicer, software version 1.41.2 (Prusa Research a.s., Prague, Czech Republic). PrusaSlicer is based on an open-source platform called Slic3r, which is licensed under the GNU Affero General Public License, version 3.

Firstly, optimal printing temperature was sought using a temperature tower test (TTT).[66] Each tower floor was printed with a different temperature. The geometrical elements present on each floor were visually evaluated and

compared as described in detail elsewhere.[66] Three towers were printed, covering temperature ranges of 220–195°C, 195–170°C and 170–150°C. The highest temperature of each aforementioned interval was recorded at the bottom of the corresponding tower, and each next floor was printed with a temperature which was 5°C lower.

Two temperatures identified by TTT were used for the warping test and fine-tuning of the printing conditions. During this test, the height of the specimen at the moment of its detachment from the printing bed was monitored, as described in our previous publications.[66] At least five testing specimens were measured.

2.6. Mechanical tests

2.6.1. Flexural test

Six standard test specimens for the three-point bending test with dimensions of 80 × 10 × 4 mm^3 were printed using optimized printing conditions for individual mixtures. Measurement was performed according to the ISO 178 standard method A using the universal testing device ZwickRoell Z010 (ZwickRoell GmbH & Co., Ulm, Germany) with a load indicator of maximum force 1 kN. The radius of the support and load was 5 mm, and the span was 64 mm. The flexural modulus was determined from the deformation range of 0.05–0.25%. The test speed was set to 2 $mm \cdot min^{-1}$ and the limit deformation to 10%.

2.6.2. Compression test

Optimized printing conditions were also used for the printing of the six standard test specimens for the compression test with dimensions of 10 × 4 × 10 mm^3. The standard ISO 604 was followed. ZwickRoell Z010 (ZwickRoell GmbH & Co., Ulm, Germany) with a load indicator of maximum force 10 kN was used. The compression modulus was determined from the deformation range of 1.25–1.50%. The test speed was 1 $mm \cdot min^{-1}$ and the limit deformation was 10%.

2.7. Biological tests

Planar testing specimens with 6 mm diameter and 1.5 mm height were printed with the surface composed of individual perimeters—the *top layer full* setting. At the same time, the granules of Mix 9, Mix 10, and Mix 15 were compression-molded to 1 mm thickness, and rounded specimens were cut out of the formed plates as a control to monitor the possible negative effect of 3D printing on the biocompatibility of the samples. All prepared scaffolds were sterilized in 70% ethanol for 30 min and then rinsed with phosphate-buffered saline (PBS) three times. Sterile scaffolds were placed into 96-well plates and 20 µL of differentiation culture medium containing 2 × 10^4 Saos-2 cells was added. The culture medium contained McCoy's medium (Sigma Aldrich) with 15% fetal bovine serum (FBS), 1% antibiotics (100 $\mu L \cdot mL^{-1}$ penicillin and 100 $\mu L \cdot mL^{-1}$ streptomycin; Sigma Aldrich), 10 nM dexamethasone (Medochemie), 2 mM β-glycerol phosphate (Sigma Aldrich) and 50 $\mu L \cdot mL^{-1}$ ascorbic acid-2-phosphate (Sigma Aldrich).

2.7.1. Metabolic activity assay

To determine the metabolic activity of the cells, metabolic activity assay (MTS) was conducted using CellTiter 96® AQueous One Solution Cell Proliferation Assay (Promega Corporation, WI, USA). The samples were transferred to clean wells and covered with 20 µL of MTS solution and 100 µL of fresh culture medium according to a standard procedure, which is already published.[62] In the control group, only the medium was aspirated and replaced with MTS solution and fresh medium. The samples were incubated in the solution for 2 h at 37°C. The absorbance was measured using an Infinite M200 PRO spectrophotometer (Tecan, Switzerland) at 490 and 690 nm wavelengths. The value measured on the sample incubated without cells was subtracted from the measured values. The value measured in the culture medium with MTS solution was subtracted from the cells on the culture plastic.

2.7.2. DNA quantification

Quantification of cellular DNA was performed using the Quant-iT™ dsDNA Assay Kit (Life Technologies). After MTS measurement, samples were placed in 200 µL lysis buffer (0.2% v/v Triton X-100, 10 mM Tris [pH 7.0], and 1 mM EDTA) and lysed in three freeze/thaw cycles, with thorough vortexing in between the cycles. During the analysis, 20 µL of cell lysate from each sample was added to 200 µL of reaction solution. The fluorescence signal intensity was measured using a fluorescence reader (Infinite M200 PRO, Tecan, Switzerland; λ_{ex} = 485 nm, λ_{em} = 523 nm). The results were evaluated using the calibration curve included in the kit.

2.7.3. Cell visualization

The distribution of cells and their shape was visualized using confocal microscopy. The samples were fixed with frozen methanol (−20°C) for 10 min. Subsequently, fluorescent probe 3,3′-diethyloxacarbocyanine iodide (DiOC6(3); 1 $\mu g \cdot mL^{-1}$ in PBS [pH 7.4]; Invitrogen) was added and incubated with the samples for 30 min at room temperature. Afterwards, propidium iodide (PI; 5 $\mu g \cdot mL^{-1}$ in PBS; Sigma Aldrich) was added for 5 min at room temperature. Subsequently, the samples were rinsed with PBS and visualized using a confocal microscope (Zeiss LSM 880 Airyscan, Oberkochen, Germany). The wavelengths used were λ_{ex} = 488 nm and λ_{em} = 520 nm for DiOC6(3) and λ_{ex} = 560 nm and λ_{em} = 580 nm for propidium iodide. Images obtained from confocal microscopy were further

used for depth cell penetration analysis. The individual images of different samples were color-coded based on their position along the Z axis. These colors correspond to the Z-axis scale in the Zeiss ZEN software, representing the position of the cells within the scaffold.

2.7.4. Alkaline phosphatase activity

Alkaline phosphatase (ALP) activity was measured as an indicator of osteogenic differentiation. The scaffolds were rinsed with PBS. Subsequently, 100 µL of ALP substrate (p-Nitrophenyl Phosphate Liquid Substrate System; Life Technologies) was added and the cells were incubated for 15 min in the dark at room temperature. After incubation, 66.6 µL of cell solution was pipetted into a new plate and 33.3 µL of 2 M NaOH solution was added to each well to stop the entire reaction. Formed ρ-nitrophenol was detected on a Synergy HT reader (BioTek Synergy HT, BioTek Instruments, Inc., USA) at a wavelength of 405 nm. The absorbance of the ALP substrate with cell carriers without cells was subtracted from the individual values.

2.7.5. Mineralization

Alizarin Red S Staining Quantification Assay kit (ARed-Q; ScienCell) was used to detect mineralization on scaffolds. Alizarin Red S forms a complex with calcium compounds in the chelation process resulting in a bright red product. After measuring ALP activity, the samples were firstly rinsed three times with PBS and then fixed in 3.6% formaldehyde (in PBS) for 15 min at room temperature. After removing the formaldehyde, the samples were rinsed three times in distilled water. The distilled water was removed and 0.1 mL of 40 mM ARS was added per well, followed by a 20-min incubation with gentle shaking. Subsequently, the samples were thoroughly rinsed in distilled water until the water was colored. Finally, the samples were photographed.

2.7.6. Statistical analysis

Six samples were used for all measurements, and at least four results were used for statistical analysis. Data were evaluated using GraphPad Prism 9.1.1. software (GraphPad Software, Boston, MA, USA). For data passing the normality test and the equality of variances test, pairwise analysis was performed using analysis of variance (ANOVA) and Tukey's comparison test for post hoc analysis. If the data were non-normally distributed, pairwise analysis was performed using Kruskal–Wallis test and Dunn's multiple comparison test for post hoc analysis. All results were considered statistically significant if $p < 0.05$.

3. Results and discussion

3.1. Thermal properties

The basic thermal properties of the prepared mixtures were characterized using DSC. The PLA used is amorphous, with a glass transition temperature of 52.2°C. Neat PHB exhibits mild T_g around 0.2°C and has a melting peak with a maximum of 172.4°C. The crystallinity of neat PHB is around 61%. In the mixtures, the glass transition of PHB was undetectable. T_g of PLA lies in the range 31–46°C and is driven by factor 3 (plasticizer content, SN/(PHB+PLA+HA)) as the only statistically significant coefficient from **Equation I** is linear (b_3). The coefficient is negative; therefore, the higher the plasticizer amount, the lower the glass transition temperature of PLA. The measured melting temperature of PHB lies between 161 and 171°C; however, no statistically significant dependency was proven. PHB crystallinity in the prepared composite mixtures was in the range of 52–64%. The statistically significant coefficient is quadratic b_{22}, which is connected to the factor 2 (HA/(PHB+PLA)). The coefficient has a negative value, thus there is a maximum of crystallinity at medium values of HA amount of the tested range.

3.2. Printability

During printing, it was verified that the edge limits of the experiment in PHB content (factor 1) and filler content (factor 2) are at the limit of the material's printability as well. The mixture with the highest amount of PHB (Mix 9) and HA (Mix 12) showed a profound brittleness and cracking during the unwinding of the filament, making them very user-unfriendly for FDM 3D printing. A suitable nozzle temperature for printing was identified by TTT and fine-tuned by warping measurement. It is important to note that this parameter combines the visual quality of the printed specimen (possible stringing, voids, or overhanging on some geometric elements) and the warping behavior; therefore, it includes both the rheology of the mixture during processing in 3D-printed extruder and the cooling behavior of the mixture. Figure 1 plots the dependence of the used printing temperature on factor 1 (PLA/PHA ratio) and factor 3 (plasticizer content), while factor 2 (HA amount) was fixed. Coefficients b_{12} and b_{23} combining the effect of filler addition with biopolymers ratio and plasticizer content, respectively, have the greatest influence on the printing temperature.

Factors 1 and 3 both have negative quadratic influences creating a dependency plane with a distinct maximum. Another significant contribution is the effects of linear coefficients related to the PLA/PHB ratio and the plasticizer content, which is evident in Figure 1B. The dependency of the printing temperature does not correlate with the PHB's melting temperature.

Generally, the primary cause of warpage during printing is thermal stresses in the printed specimen.[67] The cooling behavior and therefore the built-up residual stress of the specimen printed from amorphous and semi-

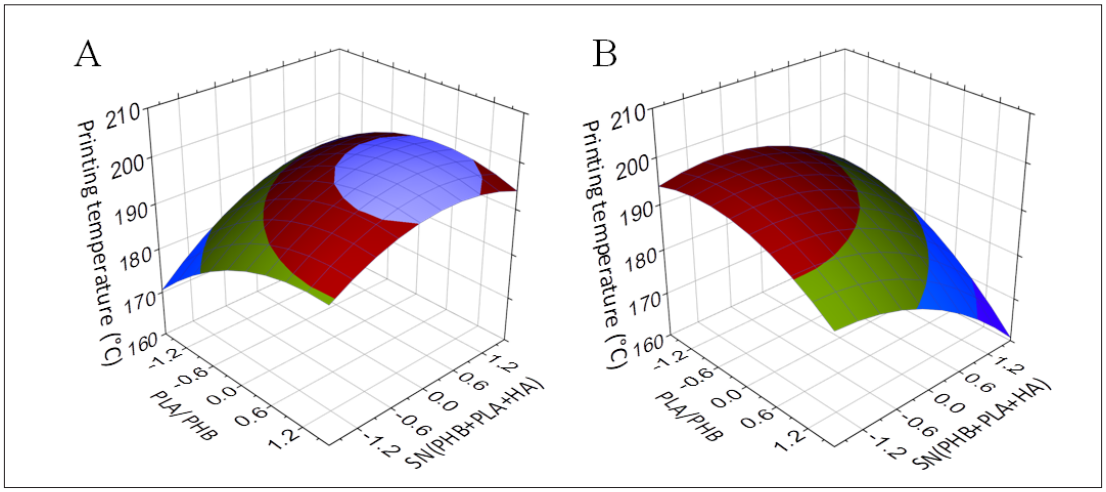

Figure 1. Printing temperature as a function of factor 1 (PHB/PLA) and factor 3 (SN/(PHB+PLA+HA)) with factor 2 (HA/(PHB+PLA)) set at the lowest amount of HA tested (A) and the highest amount of HA tested (B). Abbreviations: HA, hydroxyapatite; PHB, poly(3-hydroxybutyrate); PLA, polylactide; SN, Syncroflex™ 3114.

crystalline material differs profoundly.[68] Warping of studied mixtures can be mostly attributed to the crystallization of PHB during cooling. Therefore, it can be assumed that the higher the PHB content, the higher the warping coefficient. Indeed, the sample Mix 9 containing 70% PHB exhibited a warping coefficient of 10, meaning the testing specimen detached from the printing bed immediately upon start. Mix 7 also showed a profound warping during printing, and on the contrary, Mix 2 proved to be easy to process. Statistical evaluation supported that the PLA/PHB ratio has the major effect on warpage. A combination of linear and quadratic contribution is applied as can be seen from the graphs in Figure 2, where two plots of the dependence of the warping coefficient on factor 1 (PLA/PHA ratio) and factor 3 (plasticizer content) are shown, with a fixed value of factor 2 (HA amount). The addition of amorphous PLA content to the PHB/PLA blend reduces the warping coefficient. At the same time, due to the effect of the quadratic coefficient, there is a minimum in the dependence, which is desirable to reach. On the contrary, we can see a lower value of the warping coefficient at extreme values of the plasticizer factor, meaning around the minimum and maximum tested amount of the plasticizer. The addition of HA slightly increases the overall warping coefficient. For comparison, the warping coefficient value for commercially available PLA filament (Prusa Research, Prague, Czech Republic) is 2.9 ± 0.1. Apart from the composition of the blend, the warpage could be reduced by fine-tuning printing parameters, such as increasing the printing speed.[69]

3.3. Mechanical properties

For a successful replacement, it is important for the scaffold's mechanical properties to resemble those of the natural bone as much as possible. All materials were tested for mechanical properties under bending and compression, which simulate the stress naturally acting on a bone.

Flexural modulus and strength were evaluated, and their dependency on the most dominant composition-related factors is given in Figure 3. Flexural modulus lies in the region 2.3–3.7 GPa, the highest values were reached by Mix 4, 13, and 3, the mixtures with a high HA content and low plasticizer content. The lowest modulus was reached with Mix 5 and 6, which contain 10% of HA and 11% of the plasticizer. Statistically, all three factors significantly influence the modulus. The plasticizer content (factor 3) is the most important; the higher the SN content, the lower the modulus. On the other hand, the addition of PLA and HA has a positive effect on modulus, but the effect is 1–2 times weaker. In Figure 3A, there is the dependency of flexural modulus on factors 1 and 3 for the lowest tested amount of HA, and on the right is the dependency for the highest tested amount of HA. With the same amounts of SN and PLA/PHB ratio, only with an addition of HA, we achieve a 1 GPa modulus increase. Other statistically significant coefficients are b_{13} and b_{23} combining the influence of the plasticizer with the other two factors, which means that the plasticizer interacts not only with polymers but also with ceramic. Both are negative and reduce the flexural modulus.

The flexural strength of the measured samples is in the range of 36–59 MPa; the highest values were measured in Mix 2 and 13, followed by Mix 4. Similar to modulus, the flexural strength is mainly driven by the addition of plasticizer, which has a negative effect on this parameter, as depicted in Figure 3C and D. The second factor in

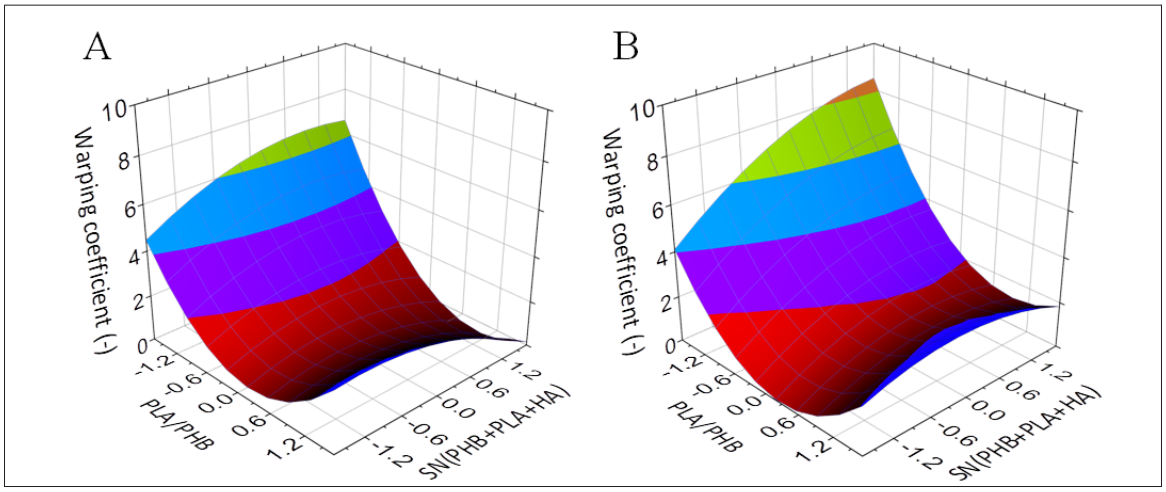

Figure 2. Warping coefficient as a function of factor 1 (PHB/PLA) and factor 3 (SN/(PHB+PLA+HA)) with factor 2 (HA/(PHB+PLA)) set at the lowest amount of HA tested (A) and the highest amount of HA tested (B). Abbreviations: HA, hydroxyapatite; PHB, poly(3-hydroxybutyrate); PLA, polylactide; SN, Syncroflex™ 3114.

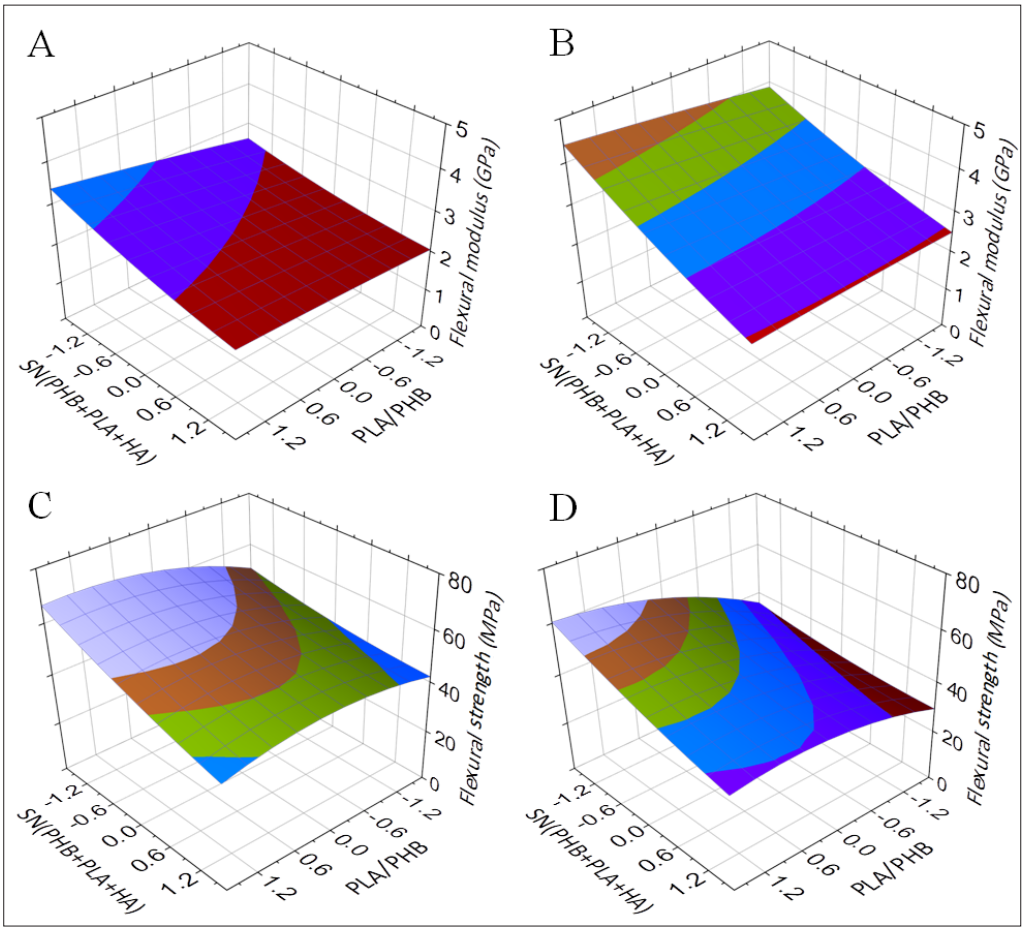

Figure 3. Flexural properties as a function of factor 3 (SN/(PHB+PLA+HA)) and factor 1 (PHB/PLA). Top panels: flexural modulus for factor 2 (HA/(PHB+PLA)) set at the lowest amount of HA tested (left) and the highest amount of HA tested (right). Bottom panels: flexural strength for factor 2 (HA/(PHB+PLA)) set at the lowest amount of HA tested (left) and the highest amount of HA tested (right). Abbreviations: HA, hydroxyapatite; PHB, poly(3-hydroxybutyrate); PLA, polylactide; SN, Syncroflex™ 3114.

relevance is the PLA/PHB ratio for which linear and quadratic coefficients are significant. Thus, the maximum flexural strength can be achieved with an intermediate PLA/PHB ratio of the tested range. The increase in HA content, although increasing the modulus, lowers the obtained flexural strength. In addition, coefficients b_{12} and b_{13} are statistically significant, therefore combining factor 1 with the two others. Practically, this means that the factors combine with each other and the effect of the addition of SN or HA differs depending on the PLA/PHB ratio.

Elastic modulus evaluated from a compression test is approximately two times lower than from a bending test, lying in the range of 0.9–1.8 GPa. The mixtures with the highest measured modulus and as well as the highest compression stress at 1% relative deformation are Mix 4 and 13. On the opposite side of the scale is Mix 6. The only two statistically significant coefficients from **Equation I** are b_2 and b_3, which relate to a linear contribution of factor 2 and factor 3, respectively. As can be also seen in Figure 4, the addition of plasticizer decreases the compression modulus while the addition of HA has a positive influence. The compressive strength of the PHA/20%β-TCP scaffold was 36.7 MPa, and 30% TCP had lower strength.[56] The compressive modulus of elasticity was recorded in the range of 0.8–1.2 GPa with a comparable trend to the compressive load capacity depending on the type of spongiosa and compaction fill. As already mentioned, the modulus of elasticity of the compact part of the bone is about 18 ± 4 GPa, while that of the porous bone in the femur region is 0.4 ± 0.3 GPa. The reported compressive strength of compact bone is 205 ± 17 MPa.[70] The considerable variance in spongiosa bone is due to the varying mineral content of the patient's bone, with a modulus variance of 50–600 MPa reported for the femoral neck.[71] Other papers also publish a mean value of the modulus of spongiosis in pressure around 100–600 MPa.[72,73] This may be due, as Gonzalez et al.[74] state, to the different temperature gradients of the printed body, which is subsequently reflected in its mechanical properties. Firstly, different crystallinity was observed in the lower and upper part of the printed body, secondly, this will also depend on the cohesion between the printed layers.[46] The presence of ceramic nanoparticles in a 3D-printed sample can lead to an improvement in its mechanical properties as long as there is no agglomeration of these nanoparticles.[75]

3.4. Biological response

Metabolic activity was measured using the MTS assay on days 1, 7, 14, and 21 of the experiment (**Figure 5**). The highest metabolic activity 24 h after placing the cells on the carriers was observed on the culture plastic (TCP), followed by the groups Mix 13 (the sample with the lowest amount of SN) and 12 (the highest amount of HA). The same applies on the 7th day of the experiment. On day 14, the metabolic activity of all 3D-printed samples was lower than for the TCP. On day 14 of the test, the values were comparable for all 3D-printed samples except for Mix 11 (the lowest amount of HA) and Mix 14 (the highest amount of SN), which exhibited the lowest metabolic activity. Although lower values were measured for Mix 15 (middle values of the composition) at the beginning of the experiment, on the 14th day, the metabolic activity was equal to that of the other groups. On day 21, the lowest metabolic activity was measured on Mix 11 and Mix 14. In

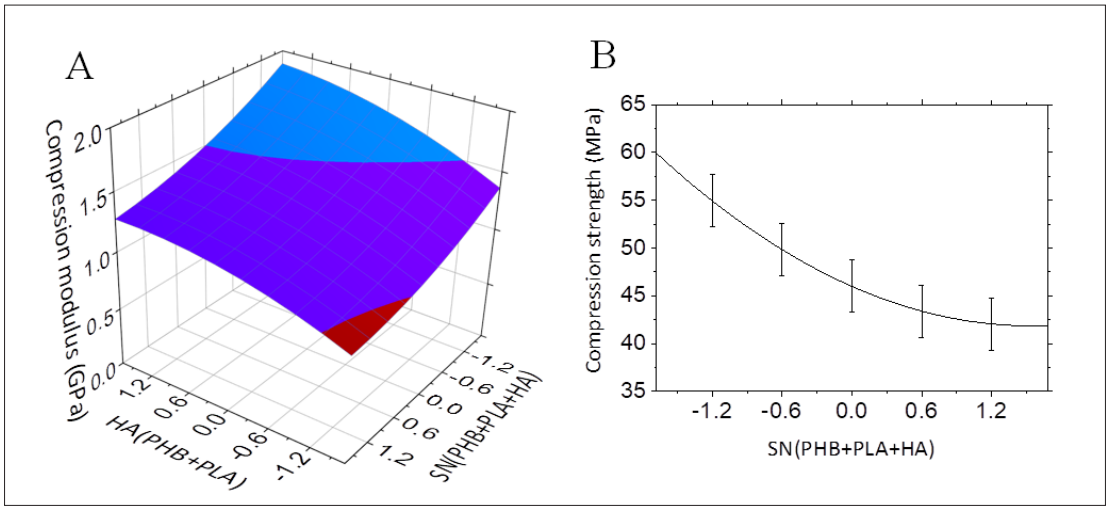

Figure 4. Compression modulus as a function of factor 3 (SN/(PHB+PLA+HA)) and factor 2 (HA/(PHB+PLA)) with factor 1 (PLA/PHB) set to an intermediate level (A), and compression strength as a function of factor 3 (B). Abbreviations: HA, hydroxyapatite; PHB, poly(3-hydroxybutyrate); PLA, Polylactide; SN, Syncroflex™ 3114.

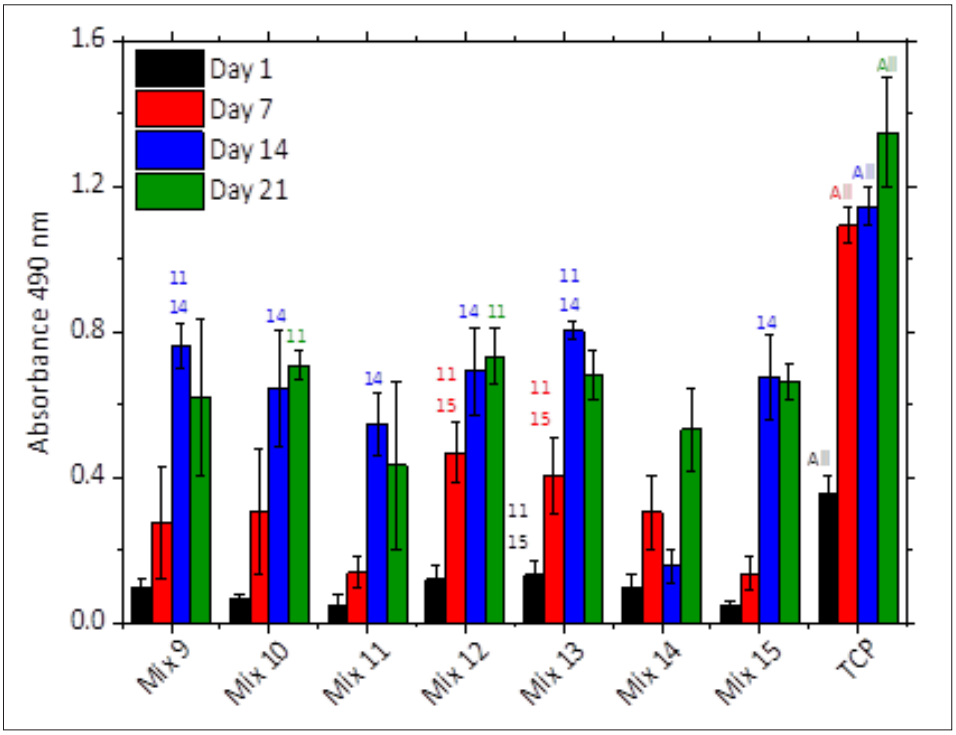

Figure 5. Metabolic activity of cells on 3D-printed supports measured by MTS. Saos-2 cells seeded on tissue culture plastic (TCP) were used as a control. A value above a column indicates that the corresponding group is significantly lower compared to the group represented by that column ($p < 0.05$, Tukey). Abbreviations: MTS, 3-(4,5-Dimethylthiazol-2-yl)-5-(3-carboxymethoxyphenyl)-2-(4-sulfophenyl)-2H-tetrazolium; TCP, tissue culture plastic.

the other groups, the absorbance was equal, but the values were lower than these measured on TCP.

Cell proliferation on 3D printed supports was measured using cellular DNA quantification (Figure 6). The highest amount of cells 24 h after deployment was observed on the culture plastic (TCP), the values were comparable on the other groups. On day 7, most cells were recorded on Mix 13, 10, and 12 scaffolds (see composition in Table 2). On the 14th day, there was a significant increase in the number of cells on Mix 13, even compared to the reference plastics. On the 21st day, there was no increase in the number of cells, and the largest amount of cells was observed on the TCP.

Cell distribution on the 3D-printed scaffolds was monitored by confocal microscopy on days 1, 7, 14, and 21 of the test (Figure 7). Cell nuclei were stained with propidium iodide (red color) and intracellular membranes by DiOC6(3) (green color). The distribution of cells was influenced by the method of cell seeding, through which the cells are seeded in a small drop of the culture medium to adhere to the scaffolds and not to be washed away from their surface. For this reason, the cell density was higher in the center of the carrier and decreased toward the sides. Therefore, it is not possible to deduct the number of cells from microscopy images. However, they reflect the results of the cell proliferation assay quite well. For example, in Mix 10 (PHB/PLA ratio 50/50), a fully confluent layer of cells was visible. On the other hand, the Mix 14 scaffold (the highest plasticizer amount) was evenly covered with cells, relatively sparsely though. On day 21, most samples were densely covered with cells. The fewest cells were observed in Mix 14. In some samples, it was evident that the cell layer had partially peeled off.

3.4.1. Osteogenic differentiation

ALP activity was measured as an indicator of osteogenic cell differentiation with results given in Figure 8. The highest ALP activity 24 h after deployment was observed on the TCP and then on the Mix 14 scaffold. On the 7th day, the highest value was measured for Mix 13 (the mixture with the lowest amount of plasticizer) and the lowest for Mix 14 (the highest amount of plasticizer). On the 14th day of the experiment, the ALP activity continued to increase for all the groups although to the least extent for Mix 14. On the 21st day, there was no further increase in ALP activity and the values were comparable among all samples.

Mineralization occurred in the late phase of cell incubation on the scaffolds as a bright red coloration, as detected on days 14 and 21 of the test (see Figure 9). It is

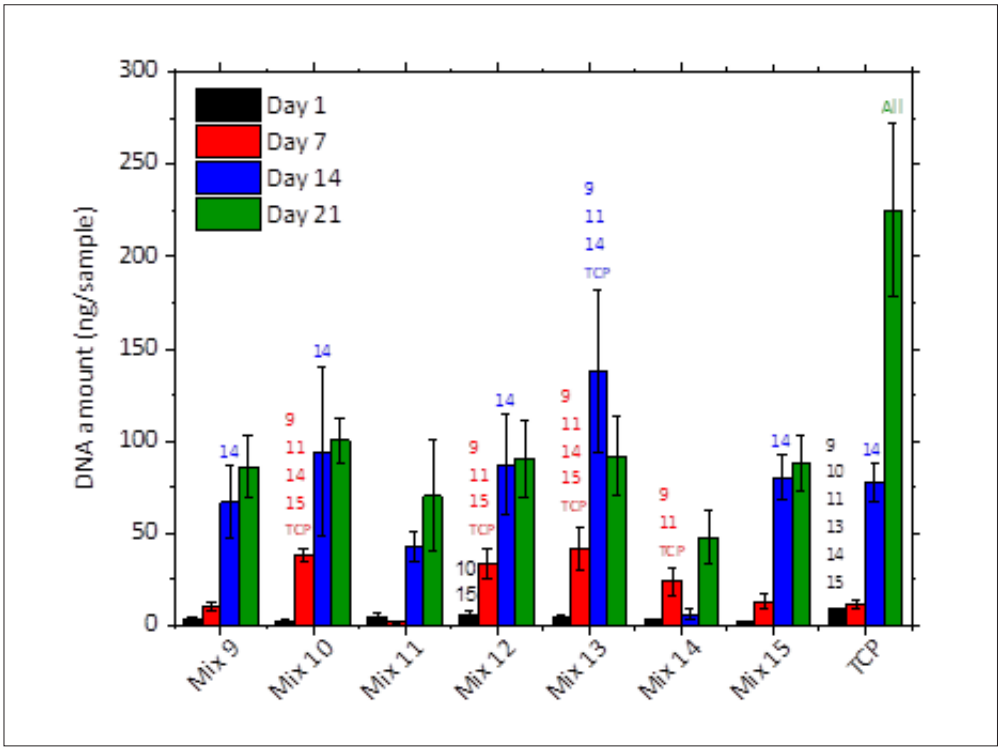

Figure 6. Cell proliferation measured by quantification of cellular DNA. Saos-2 cells seeded on culture plastic (TCP) were used as a control. A value above a column indicates that the corresponding group is significantly lower compared to the group represented by that column ($p < 0.05$, Tukey). Abbreviations: TCP, tissue culture plastic.

evident that the greatest degree of mineralization occurred on Mix 12. On the contrary, we observed a low level of staining on Mix 14. However, there was a large variability between individual samples. On the 21st day, there was an increase in mineralization indicated by more distinct staining, especially in Mix 10, 11, 12, 13, and 15 samples. The lowest mineralization level was observed in Mix 14, which corresponds to a smaller number of cells.

3.5. Optimized blend

From the results, it is possible to find the composition of the mixture within the tested range, which should have the most suitable properties for bone tissue engineering, namely the best printability and maximum mechanical properties. Four mixture compositions fulfilling the following optimization criteria were obtained: minimum warping coefficient; maximum flexural strength; maximum compression modulus; and maximum compression modulus with a warping coefficient of no more than one at the same time.

The fourth mixture is supposed to have an optimal ratio between the printability and mechanical properties and at the same time contains a high amount of bioactive filler, which is important for the biological response. The precise formula of this mixture is 35.2% PHB, 30.8% PLA, 28.3% HA, and 5.6% SN and was named an "optimized" mixture. The compressive strength of compact and trabecular bone is 205 ± 17 and 6.8 ± 4.8 MPa, respectively. The compression modulus of the compact part of the bone is around 18 ± 4 GPa, and for trabecular bone in the femur region, it is 0.4 ± 0.3 GPa.[70] Considerable variance in cancellous bone is due to the different mineral content in the patient's bone; for the femur neck, the modulus variance is from 50 to 600 MPa.[71] Other works have also reported the mean value of the modulus of elasticity in the compression of porous bone at around 100–600 MPa.[72,73,76] Wurm et al.[26] successfully employed FDM for the fabrication of PLA discs and the influence of processing technique upon the biocompatibility of printed parts was assessed. *In vitro* tests using human fetal osteoblasts showed no cytotoxic effects of PLA discs. Since FDM proved no negative influence on the biocompatibility of PLA, this 3D-printing technique could be further used in reconstructive surgery for the production of individual-shaped scaffolds or other implants.[26] PLA modulus encompasses over the range of 10–900 MPa, which spans the complete range of substrate moduli for trabecular bone (93–365 MPa) and the lower end of the range for cortical bone (87–500 MPa).[77] Osteogenic differentiation and mineralization increased as the substrate modulus increased from 10 to 900 MPa(Table 3).[78]

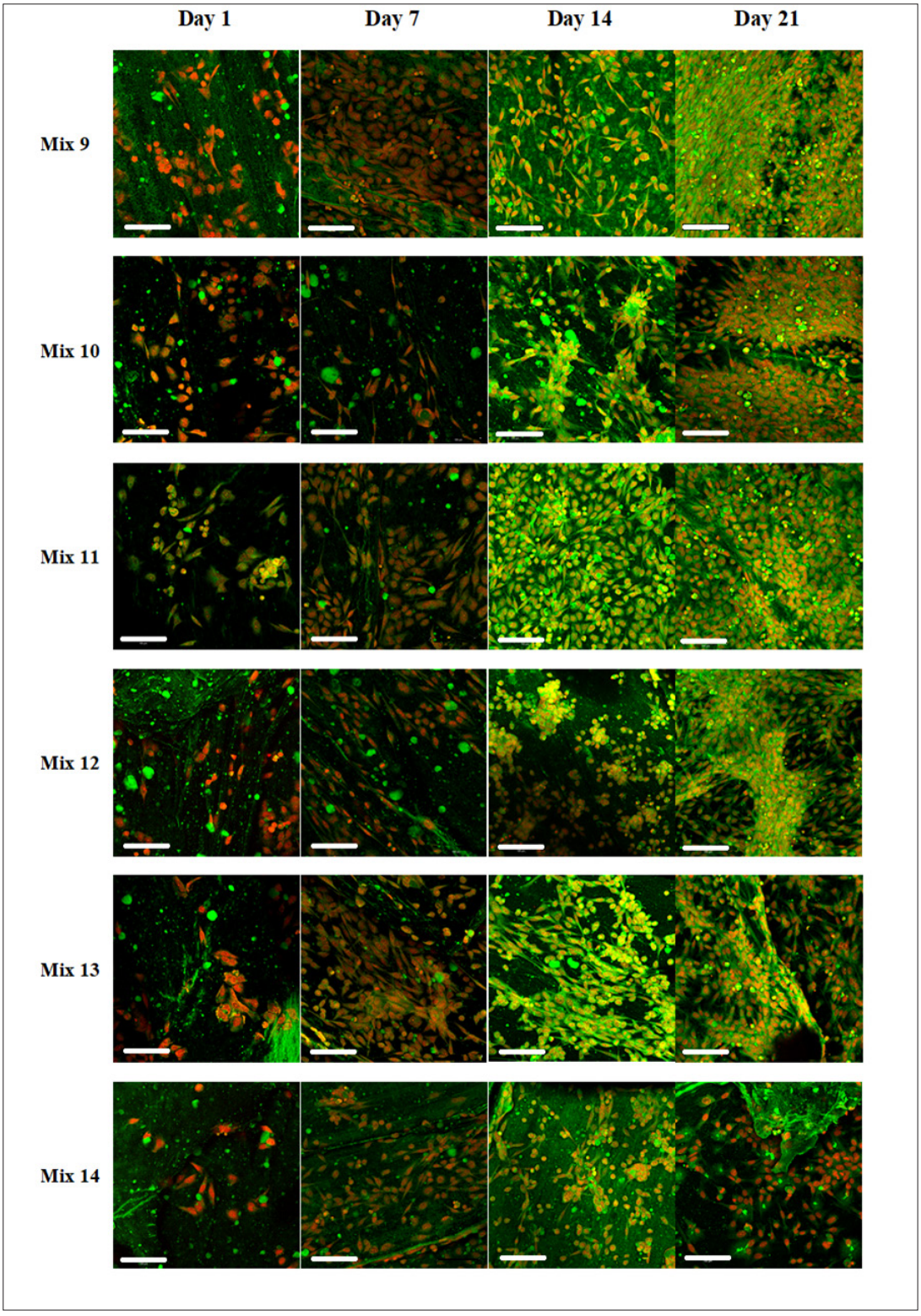

Figure 7. Cell adhesion and proliferation on the carriers on day 1, 7, 14, and 21. Cell nuclei were stained with propidium iodide (red), intracellular membranes with DiOC6(3) (green). Scale bar: 100 μm.

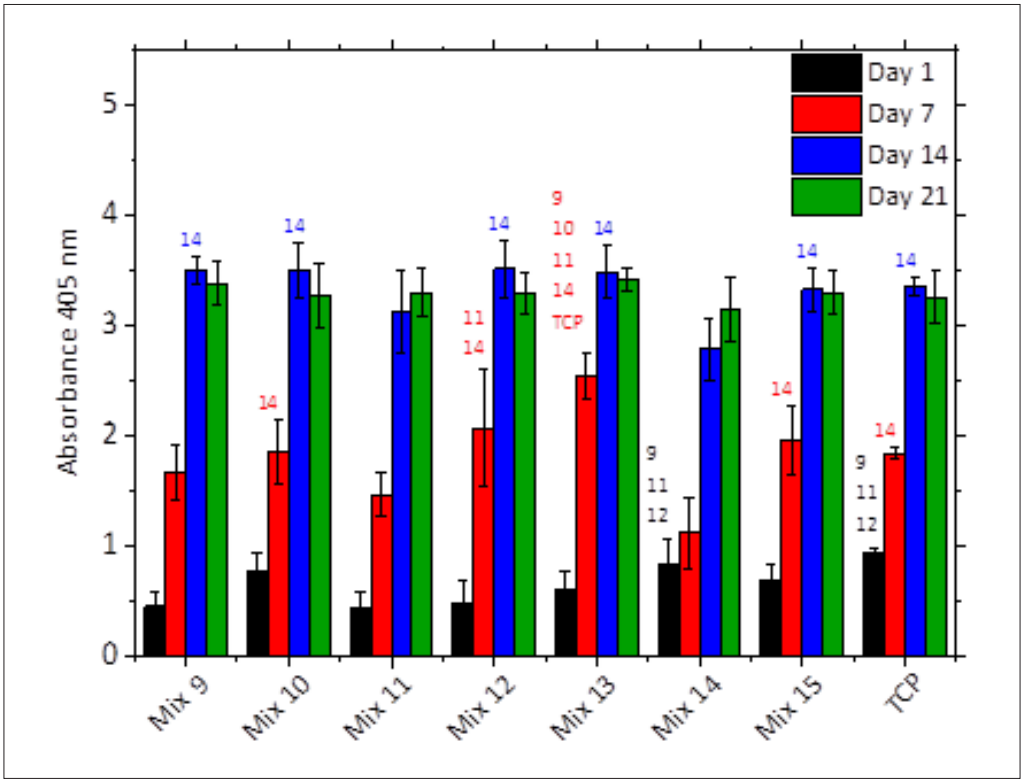

Figure 8. Alkaline phosphatase activity was measured as an indicator of osteogenic differentiation. Saos-2 cells seeded on culture plastic (TCP) were used as a control. A value above a column indicates that the corresponding group is significantly lower compared to the group represented by that column ($p < 0.05$, Tukey). Abbreviations: TCP, tissue culture plastic .

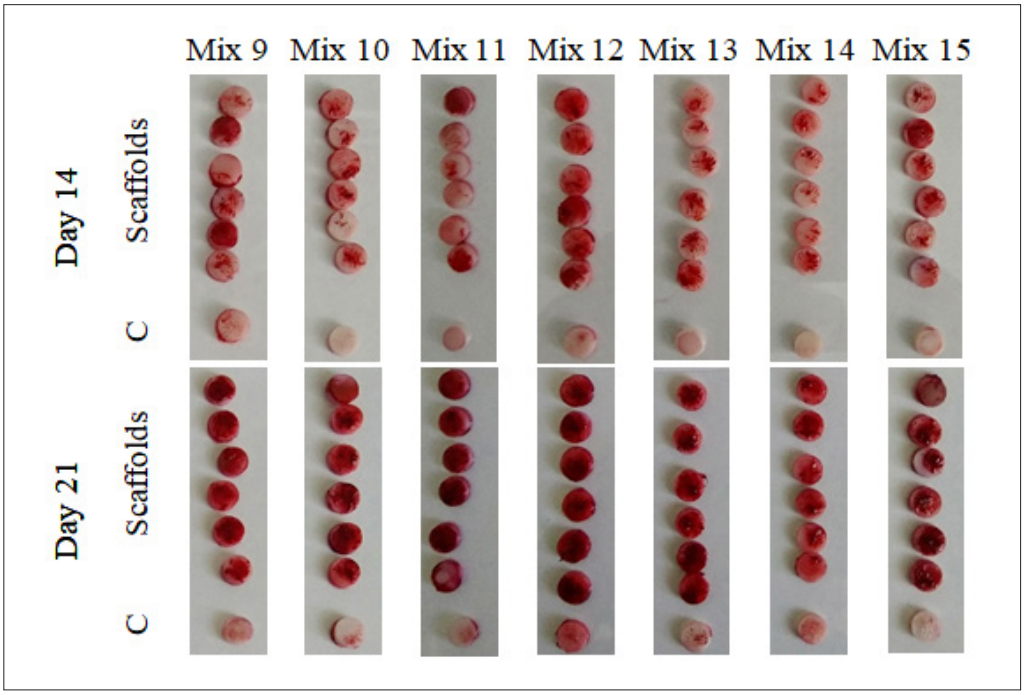

Figure 9. Mineralization on scaffolds detected with Alizarin Red S assay. Positive red staining indicates mineralization produced by the seeded Saos2 cells. Six samples were measured, and the samples in the last (7th) row are controls (C) without cells.

Table 3. The composition and theoretical properties of optimized blends.

	Composition (%)				Theoretical properties					
	PHB	PLA	HA	SN	Printing temperature (°C)	Warping coefficient (-)	Flexural modulus (GPa)	Flexural strength (MPa)	Compression modulus (GPa)	Stress at 1% deformation (MPa)
1	56	34	5	6	186.8	0.5[a]	3.1	64.9	1.4	6.3
2	48	42	5	6	189.4	1.7	3.3	66.9[a]	1.4	6.2
3	33	33	28	6	184.4	2.1	4.4	60.5	2.4[a]	15.2
4	35	31	28	6	188.2	1.0[a]	4.3	59.7	2.3[a]	14.1

[a] Optimized property.
Abbreviations: HA, hydroxyapatite; PHB, poly(3-hydroxybutyrate); PLA, polylactide; SN, Syncroflex™ 3114.

4. Conclusion

In conclusion, this study is aimed at the preparation and characterization of material properties of PHB-based composite blends, which are suitable for use in tissue engineering. The blends were processed into 3D-printing filaments and tested in terms of their printability, thermal and mechanical properties, and biological response. Biological properties were studied for 21 days on the mixtures with one of the four components in a limited amount within the scope of the experiment. All the 3D-printed scaffolds were biocompatible, and the cells adhered to the carriers had a good morphology. On day 21, there was no longer an increase in the number of cells, nor an increase in ALP activity. On the contrary, it was noticeable that there was an increase in mineralization. The highest metabolic activity, proliferation and rate of osteogenic differentiation were observed on the sample with the lowest amount of plasticizer (Mix 13) followed by the mixture containing the highest amount of bioactive hydroxyapatite (Mix 12). In contrast, the worst results were observed for the sample with the highest plasticizer content (Mix 14). Overall, our results show that PHB-based composite blends hold a great potential for tissue engineering applications. By adopting the design of experiment, we obtained four mixture compositions with minimum warping coefficient, maximum flexural strength, maximum compression modulus, and maximum compression modulus with a warping coefficient of no more than one at the same time.

Acknowledgments

None

Funding

Thee authors acknowledge the support from projects "New circular biotechnologies and biomedical applications" No. CZ.01.1.02/0.0/0.0/20_321/002 4676; "Excellence in regenerative medicine" No. CZ.02.01.01/00/22_008/0004562 and from Operational Program Integrated Infrastructure for the project "Center for Medical Bioadditive Research and Production (CEMBAM), code ITMS2014 +: 313011V358, co-financed by the European Regional Development Fund."

Conflict of interest

The authors declare they have no competing interests.

Author contributions

Conceptualization: Veronika Melčová, Radek Přikryl
Data curation: Veronika Melčová, Přemysl Menčík, Štěpán Krobot, Ján Bočkaj, Pavol Alexy
Formal analysis: Přemysl Menčík, Ján Bočkaj, Sára Vach Agócsová, Štěpán Krobot, Kateřina Chaloupková, Věra Hedvičáková
Funding acquisition: Radek Přikryl, Pavol Alexy, Michala Klusáček Rampichová
Investigation: Přemysl Menčík, Štěpán Krobot, Veronika Melčová, Kateřina Chaloupková, Věra Hedvičáková
Methodology: Veronika Melčová, Radek Přikryl, Michala Klusáček Rampichová
Project administration: Veronika Melčová
Supervision: Veronika Melčová, Radek Přikryl
Writing – original draft: Štěpán Krobot, Veronika Melčová
Writing – review & editing: Veronika Melčová, Štěpán Krobot, Michala Klusáček Rampichová

Ethics approval and consent to participate

Not applicable.

Consent for publication

Not applicable.

Availability of data

Data are available from the corresponding author upon reasonable request.

References

1. Abbasi N, Hamlet S, Love RM, Nguyen N.-T. Porous scaffolds for bone regeneration. *J Sci Adv Mater Devices.* 2020;5(1):1-9. doi: 10.1016/j.jsamd.2020.01.007
2. Ngo TD, Kashani A, Imbalzano G, Nguyen KTQ, Hui D. Additive manufacturing (3D printing): a review of materials, methods, applications and challenges. *Compos B Eng.* 2018;143:172-196. doi: 10.1016/j.compositesb.2018.02.012
3. Zhang Q, Zhou J, Zhi P, et al. 3D printing method for bone tissue engineering scaffold. *Med Nov Technol Devices.* 2023;17:100205. doi: 10.1016/j.medntd.2022.100205
4. Bose S, Vahabzadeh S, Bandyopadhyay A. Bone tissue engineering using 3D printing. *Mater Today*. 2013;16(12):496-504. doi: 10.1016/j.mattod.2013.11.017
5. Chiulan I, Frone AN, Brandabur C, Panaitescu DM. Recent advances in 3D printing of aliphatic polyesters. *Bioeng Basel Switz* 2017;5(1):E2. doi: 10.3390/bioengineering5010002
6. Shunmugasundaram M, Baig M, Madala A. A review of bio-degradable materials for fused deposition modeling machine. *Mater Today Proc.* 2020;27:1596-1600. doi: 10.1016/j.matpr.2020.03.267
7. Mehrpouya M, Vahabi H, Barletta M, Laheurte P, Langlois V. Additive manufacturing of polyhydroxyalkanoates (PHAs) biopolymers: materials, printing techniques, and applications. *Mater Sci Eng C Mater Biol Appl.* 2021;127:112216. doi: 10.1016/j.msec.2021.112216
8. Amrita, Manoj A, Panda RC. Biodegradable filament for 3D printing process: a review. *Eng Sci.* 2022;18(7):11-19. doi: 10.30919/es8d616
9. Rigotti D, Pegoretti A. Additive manufacturing with biodegradable polymers. In: *Biodegradable Polymers, Blends and Composites*. Woodhead Publishing; 2022:611-679. doi: 10.1016/B978-0-12-823791-5.00026-0.
10. Hutmacher DW, Schantz T, Zein I, Ng KW, Teoh SH, Tan KC. Mechanical properties and cell cultural response of polycaprolactone scaffolds designed and fabricated via fused deposition modeling. *J Biomed Mater Res.* 2001;*55*(2):203-216. doi: 10.1002/1097-4636(200105)55:2<203::AID-JBM1007>3.0.CO;2-7
11. Xiong Z, Yan Y, Zhang R, Sun L. Fabrication of porous poly(l-Lactic Acid) scaffolds for bone tissue engineering via precise extrusion. *Scr Mater.* 2001;45(7):773-779. doi: 10.1016/S1359-6462(01)01094-6.
12. Zein I, Hutmacher DW, Tan KC, Teoh SH. Fused deposition modeling of novel scaffold architectures for tissue engineering applications. *Biomaterials.* 2002;23(4):1169-1185. doi: 10.1016/S0142-9612(01)00232-0
13. Cao T, Ho K-H, Teoh S-H. Scaffold design and in vitro study of osteochondral coculture in a three-dimensional porous polycaprolactone scaffold fabricated by fused deposition modeling. *Tissue Eng.* 2003;9(Suppl 1):S103-S112. doi: 10.1089/10763270360697012
14. Park S, Kim G, Jeon YC, Koh Y, Kim W. 3D polycaprolactone scaffolds with controlled pore structure using a rapid prototyping system. *J Mater Sci Mater Med.* 2009;20(1):229-234. doi: 10.1007/s10856-008-3573-4
15. Domingos M, Chiellini F, Gloria A, Ambrosio L, Bartolo P, Chiellini E. Effect of process parameters on the morphological and mechanical properties of 3D bioextruded poly(E-caprolactone) scaffolds. *Rapid Prototyp J.* 2012;18(1): 56-67. doi: 10.1108/13552541211193502
16. Korpela J, Kokkari A, Korhonen H, Malin M, Närhi T, Seppälä J. Biodegradable and bioactive porous scaffold structures prepared using fused deposition modeling. *J Biomed Mater Res B Appl Biomater.* 2013;*101B*(4):610-619. doi: 10.1002/jbm.b.32863
17. Rai B, Teoh SH, Ho KH, et al. The effect of rhBMP-2 on canine osteoblasts seeded onto 3D bioactive polycaprolactone scaffolds. *Biomaterials.* 2004;25(24):5499-5506. doi: 10.1016/j.biomaterials.2004.01.007
18. Rai B, Lin JL, Lim ZXH, Guldberg RE, Hutmacher DW, Cool SM. Differences between in vitro viability and differentiation and in vivo bone-forming efficacy of human mesenchymal stem cells cultured on PCL–TCP scaffolds. *Biomaterials.* 2010;31(31):7960-7970. doi: 10.1016/j.biomaterials.2010.07.001
19. Teo EY, Ong S-Y, Chong MSK, et al. Polycaprolactone-based fused deposition modeled mesh for delivery of antibacterial agents to infected wounds. *Biomaterials.* 2011;32(1):279–287. doi: 10.1016/j.biomaterials.2010.08.089
20. Konopnicki S, Sharaf B, Resnick C., et al. Tissue-engineered bone with 3-dimensionally printed β-tricalcium phosphate and polycaprolactone scaffolds and early implantation: an in vivo pilot study in a porcine mandible model. *J Oral Maxillofac Surg.* 2015;73(5):1016.e1-1016.e11. doi: 10.1016/j.joms.2015.01.021
21. Dávila JL, Freitas MS, Inforçatti Neto P, Silveira ZC, Silva JVL, d'Ávila MA. Fabrication of PCL/β-TCP scaffolds by 3d mini-screw extrusion printing. *J Appl Polym Sci.* 2016;133(15):1-9. doi: 10.1002/app.43031
22. Sparks DS, Wiper J, Lloyd T, et al. Protocol for the BONE-RECON trial: a single-arm feasibility trial for critical sized lower limb BONE defect RECONstruction using the mPCL-TCP scaffold system with autologous vascularised corticoperiosteal tissue transfer. *BMJ Open.* 2023;13(5):e056440.

doi: 10.1136/bmjopen-2021-056440

23. *Next-level tissue regeneration*. Biomendex. https://biomendex.com/(accessed 2024-09-19).

24. Chen X, Chen G, Wang G, Zhu P, Gao C. Recent progress on 3D-printed polylactic acid and its applications in bone repair. *Adv Eng Mater.* 2020;22(4):1901065. doi: 10.1002/adem.201901065

25. Gregor A, Filová E, Novák M, et al. Designing of PLA scaffolds for bone tissue replacement fabricated by ordinary commercial 3D printer. *J Biol Eng.* 2017;11:31. doi: 10.1186/s13036-017-0074-3

26. Wurm MC, Möst T, Bergauer B, et al. In-vitro evaluation of polylactic acid (PLA) manufactured by fused deposition modeling. *J Biol Eng.* 2017;11(1):29. doi: 10.1186/s13036-017-0073-4

27. Germain L, Fuentes CA, van Vuure AW, Rieux Ad, Dupont-Gllain C. 3D-printed biodegradable gyroid scaffolds for tissue engineering applications. *Mater Des.* 2018;151:113-122. doi: 10.1016/j.matdes.2018.04.037

28. Alizadeh-Osgouei M, Li Y, Vahid A, Ataee A, Wen C. High strength porous PLA gyroid scaffolds manufactured via fused deposition modeling for tissue-engineering applications. *Smart Mater Med.* 2021;*2*:15-25. doi: 10.1016/j.smaim.2020.10.003

29. Eryildiz M. Fabrication of drug-loaded 3D-printed bone scaffolds with radial gradient porosity. *J Mater Eng Perform.* 2023;32(9):4249-4257. doi: 10.1007/s11665-022-07490-0

30. Schoen AH. *Infinite Periodic Minimal Surfaces Without Self-Intersections*. National Aeronautics and Space Administration; 1970.

31. Xiong Z, Yan Y, Wang S, Zhang R, Zhnag C. Fabrication of porous scaffolds for bone tissue engineering via low-temperature deposition. *Scr Mater.* 2002;46(11):771-776. doi: 10.1016/S1359-6462(02)00071-4

32. Drummer D, Cifuentes-Cuéllar S, Rietzel D. Suitability of PLA/TCP for fused deposition modeling. *Rapid Prototyp J.* 2012;18(6):500-507. doi: 10.1108/13552541211272045

33. Elhattab K, Bhaduri SB, Sikder P. Influence of fused deposition modelling nozzle temperature on the rheology and mechanical properties of 3D printed β-tricalcium phosphate (TCP)/polylactic acid (PLA) composite. *Polymers.* 2022;14(6):1222. doi: 10.3390/polym14061222

34. Distler T, Fournier N, Grünewald A, et al. Polymer-bioactive glass composite filaments for 3D scaffold manufacturing by fused deposition modeling: fabrication and characterization. *Front Bioeng Biotechnol.* 2020;8:552. doi: 10.3389/fbioe.2020.00552

35. Matsuo A, Chiba H, Takahashi H, Toyoda J, Abukawa H. Clinical application of a custom-made bioresorbable raw particulate hydroxyapatite/poly-l-lactide mesh tray for mandibular reconstruction. *Odontology.* 2010;98(1):85-88. doi: 10.1007/s10266-009-0111-x

36. Senatov FS, Niaza KV, Stepashkin AA, Kaloshkin SD. Low-cycle fatigue behavior of 3d-printed PLA-based porous scaffolds. *Compos Part B Eng.* 2016;97:193-200. doi: 10.1016/j.compositesb.2016.04.067

37. Esposito Corcione C, Gervaso F, Scalera F, Montagna F, Sannino A, Maffezzoli A. The feasibility of printing polylactic acid–nanohydroxyapatite composites using a low-cost fused deposition modeling 3D printer. *J Appl Polym Sci.* 2017;134(13);44656. doi: 10.1002/app.44656

38. Esposito Corcione C, Scalera F, Gervaso F, Montagna F, Sannino A, Maffezzoli A. One-step solvent-free process for the fabrication of high loaded PLA/HA composite filament for 3D printing. *J Therm Anal Calorim.* 2018;134(1):575-582. doi: 10.1007/s10973-018-7155-5

39. Esmaeili S, Akbari Aghdam H, Motififard M, et al. A porous polymeric–hydroxyapatite scaffold used for femur fractures treatment: fabrication, analysis, and simulation. *Eur J Orthop Surg Traumatol.* 2020;30(1):123-131. doi: 10.1007/s00590-019-02530-3

40. Dubinenko G, Zinoviev A, Bolbasov E, et al. Highly filled poly(l-lactic acid)/hydroxyapatite composite for 3D printing of personalized bone tissue engineering scaffolds. *J Appl Polym Sci.* 2021;138(2):49662. doi: 10.1002/app.49662

41. Alves AA, Siqueira EC, Barros MPS, Silva PEC, Houllou LM. Polyhydroxyalkanoates: a review of microbial production and technology application. *Int J Environ Sci Technol.* 2023;20(3):3409-3420. doi: 10.1007/s13762-022-04213-9

42. Kosorn W, Sakulsumbat M, Uppanan P, et al. PCL/PHBV blended three dimensional scaffolds fabricated by fused deposition modeling and responses of chondrocytes to the scaffolds. *J Biomed Mater Res B Appl Biomater.* 2017;105(5):1141-1150. doi: 10.1002/jbm.b.33658

43. Ausejo JG, Rydz J, Musiol M, et al. A comparative study of three-dimensional printing directions: the degradation and toxicological profile of a PLA/PHA blend. Polym Degrad Stab. 2018;152:191-207. doi: 10.1016/j.polymdegradstab.2018.04.024

44. Findrik Balogová A, Hudák R, Tóth T, et al. Determination of geometrical and viscoelastic properties of PLA/PHB samples made by additive manufacturing for urethral substitution. *J Biotechnol.* 2018;284:123-130. doi: 10.1016/j.jbiotec.2018.08.019

45. Ecker JV, Burzic I, Haider A, Hild S, Rennhofer H. Improving the impact strength of PLA and its blends with PHA in fused layer modelling. *Polym Test.* 2019;78:105929. doi: 10.1016/j.polymertesting.2019.105929

46. Rydz J, Włodarczyk J, Gonzalez Ausejo J, et al. Three-dimensional printed PLA and PLA/PHA dumbbell-shaped specimens: material defects and their impact on degradation behavior. *Materials.* 2020;13(8):2005. doi: 10.3390/ma13082005

47. Findrik Balogová A, Trebuňová M, Ižaríková G, et al. In vitro degradation of specimens produced from PLA/PHB by additive manufacturing in simulated conditions. *Polymers.* 2021;13(10):1542. doi: 10.3390/polym13101542

48. Gielisch M, Heimes D, Thiem DGE, et al. Steam-sterilized and degradable fused filament fabrication-printed polylactide/ polyhydroxyalkanoate surgical guides for dental implants: are they accurate enough for static navigation? *Int J Bioprint.* 2022;9(2):655. doi: 10.18063/ijb.v9i2.655

49. Kohan M, Lancoš S, Schnitzer M, Živčák J, Hudák R. Analysis of PLA/PHB biopolymer material with admixture of hydroxyapatite and tricalcium phosphate for clinical use. *Polymers.* 2022;14(24):5357. doi: 10.3390/polym14245357

50. Giubilini A, Siqueira G, Clemens FJ, et al. 3D-printing nanocellulose-poly(3-hydroxybutyrate-Co-3-hydroxyhexanoate) biodegradable composites by fused deposition modeling. *ACS Sustain Chem Eng.* 2020;8(27):10292-10302. doi: 10.1021/acssuschemeng.0c03385

51. Kovalcik A, Sangroniz L, Kalina M, et al. Properties of scaffolds prepared by fused deposition modeling of poly(hydroxyalkanoates). *Int J Biol Macromol.* 2020;161:364-376. doi: 10.1016/j.ijbiomac.2020.06.022

52. Dong X, Premaratne ID, Sariibrahimoglu K, Limem S, Scott J, Gadjiko M. 3D-printed poly-4-hydroxybutyrate bioabsorbable scaffolds for nipple reconstruction. *Acta Biomater.* 2022;143:333-343. doi: 10.1016/j.actbio.2022.02.040

53. Volpini V, Giubilini A, Corsi L, Nobili A, Bondioli F. Characterization of biocompatible scaffolds manufactured by fused filament fabrication of poly(3-Hydroxybutyrate-Co-3-Hydroxyhexanoate). R Soc Open Sci. 2022;9(4): 211485. doi: 10.1098/rsos.211485

54. Ivorra-Martinez J, Peydro MÁ, Gomez-Caturla J, Sanchez-Nacher L, Boronat T, Balart R. The effects of processing parameters on mechanical properties of 3D-printed polyhydroxyalkanoates parts. *Virtual Phys Prototyp.* 2023;18(1):e2164734. doi: 10.1080/17452759.2022.2164734

55. Aráoz B, Karakaya E, Wusener AG, et al. 3D printed poly(Hydroxybutyrate-Co-Hydroxyvalerate)—45S5 bioactive glass composite resorbable scaffolds suitable for bone regeneration. *J Mater Res.* 2021;36:4000-4012. doi: 10.1557/s43578-021-00272-9

56. Ye X, Zhang Y, Liu T, et al. Beta-tricalcium phosphate enhanced mechanical and biological properties of 3D-printed polyhydroxyalkanoates scaffold for bone tissue engineering. *Int J Biol Macromol.* 2022;209:1553-1561. doi: 10.1016/j.ijbiomac.2022.04.056

57. Chen G-Q, Wu Q. The application of polyhydroxyalkanoates as tissue engineering materials. *Biomaterials.* 2005;26(33):6565-6578. doi: 10.1016/j.biomaterials.2005.04.036

58. Lim J, You M, Li J, Li Z. Emerging bone tissue engineering via polyhydroxyalkanoate (PHA)-based scaffolds. *Mater Sci Eng C Mater Biol Appl.* 2017;79:917-929. doi: 10.1016/j.msec.2017.05.132

59. Butt FI, Muhammad N, Hamid A, Moniruzzaman M, Sharif F. Recent progress in the utilization of biosynthesized polyhydroxyalkanoates for biomedical applications - review. *Int J Biol Macromol.* 2018;120(Pt A): 1294-1305. doi: 10.1016/j.ijbiomac.2018.09.002

60. Gregory DA, Taylor CS, Fricker AT, et al. Polyhydroxyalkanoates and their advances for biomedical applications. *Trends Mol Med.* 2022;28(4):331-342. doi: 10.1016/j.molmed.2022.01.007

61. Pereira TF, Oliveira MF, Maia IA, et al. 3D printing of poly(3-Hydroxybutyrate) porous structures using selective laser sintering. *Macromol Symp.* 2012;319(1):64-73. doi: 10.1002/masy.201100237

62. Melčová V, Svoradová K, Menčík P, et al. FDM 3D printed composites for bone tissue engineering based on plasticized Poly(3-Hydroxybutyrate)/Poly(d,l-Lactide) Blends. *Polymers.* 2020;12(12):2806. doi: 10.3390/polym12122806

63. Krobot Š, Melčová V, Menčík P, et al. Poly(3-Hydroxybutyrate) (PHB) and polycaprolactone (PCL) based blends for tissue engineering and bone medical applications processed by FDM 3D printing. *Polymers.* 2023;15(10):2404. doi: 10.3390/polym15102404

64. Kanabenja W, Passarapark K, Subchokpool T, et al. 3D printing filaments from plasticized polyhydroxybutyrate/ polylactic acid blends reinforced with hydroxyapatite. *Addit Manuf.* 2022;59:103130. doi: 10.1016/j.addma.2022.103130

65. Moroni S, Khorshid S, Aluigi A, Tiboni M, Casettari L. Poly(3-Hydroxybutyrate): a potential biodegradable excipient for direct 3D printing of pharmaceuticals. *Int J Pharm.* 2022;623:121960. doi: 10.1016/j.ijpharm.2022.121960

66. Kontárová S, Přikryl R, Melčová V, et al. Printability, mechanical and thermal properties of poly(3-Hydroxybutyrate)-Poly(Lactic Acid)-plasticizer blends for three-dimensional (3D) printing. *Materials.* 2020;13(21):4736. doi: 10.3390/ma13214736

67. Armillotta A, Bellotti M, Cavallaro M. Warpage of FDM parts: experimental tests and analytic model. *Robot Comput-Integr Manuf.* **2018**;50:140-152. doi: 10.1016/j.rcim.2017.09.007

68. Antony Samy A, Golbang A, Harkin-Jones E, Archer E, Dahale M, McIlhagger A. Influence of ambient temperature on part distortion: a simulation study on amorphous and semi-crystalline polymer. *Polymers.* 2022;14(5):879. doi: 10.3390/polym14050879

69. Samy AA, Golbang A, Harkin-Jones E, Archer E, Tormey D, McIlhagger A. Finite element analysis of residual stress and warpage in a 3D printed semi-crystalline polymer: effect of ambient temperature and nozzle speed. *J Manuf Process.* 2021;70:389-399. doi: 10.1016/j.jmapro.2021.08.054

70. Wang X, Xu S, Zhou S, et al. Topological design and additive manufacturing of porous metals for bone scaffolds and orthopaedic implants: a review. *Biomaterials.* 2016;83:127-141. doi: 10.1016/j.biomaterials.2016.01.012

71. Haba Y, Skripitz R, Lindner T, et al. Bone mineral densities and mechanical properties of retrieved femoral bone samples in relation to bone mineral densities measured in the respective patients. *ScientificWorldJournal* 2012;2012:242403. doi: 10.1100/2012/242403

72. Rohlmann A, Zilch H, Bergmann G, Kolbel R. Material properties of femoral cancellous bone in axial loading. *Arch. Orthop Trauma Surg.* 1980;97(2); 95-102. doi: 10.1007/BF00450930

73. Uchiyama T, Tanizawa T, Muramatsu H, Endo N, Takahashi HE, Hara T. Three-dimensional microstructural analysis of human trabecular bone in relation to its mechanical properties. Bone. 1999;25(4):487-491. doi: 10.1016/S8756-3282(99)00188-X

74. Gonzalez Ausejo J, Rydz J, Musioł M, et al. Three-dimensional printing of PLA and PLA/PHA dumbbell-shaped specimens of crisscross and transverse patterns as promising materials in emerging application areas: prediction study. *Polym Degrad Stab.* 2018;156:100-110. doi: 10.1016/j.polymdegradstab.2018.08.008

75. Ayatollahi MR, Nemati Giv A, Razavi N, Khoramishad, H. Mechanical properties of adhesively single lap-bonded joints reinforced with multi-walled carbon nanotubes and silica nanoparticles. *J Adhes.* 2017; *93*(11): 896-913. doi: 10.1080/00218464.2016.1187069

76. Zilch H, Rohlmann A, Bergmann G, Kölbel R. Material properties of femoral cancellous bone in axial loading. Part II: time dependent properties. *Arch Orthop Trauma Surg (1978).* 1980;97(4):257-262. doi: 10.1007/BF00380706

77. Song Y, Li Y, Song W, Yee K, Lee K-Y, Tagarielli VL. Measurements of the mechanical response of unidirectional 3D-printed PLA. *Mater Des.* 2017;123:154-164. doi: 10.1016/j.matdes.2017.03.051

78. Guo R, Lu S, Page JM, et al. Fabrication of 3D scaffolds with precisely controlled substrate modulus and pore size by templated-fused deposition modeling to direct osteogenic differentiation. *Adv Healthc Mater.* 2015;4(12): 1826-1832. doi: 10.1002/adhm.201500099